What prevents nitrogen depletion in the OMZ of the Eastern Tropical South Pacific?

B. Su, M. Pahlow, H. Wagner, and A. Oschlies

GEOMAR Helmholtz Centre for Ocean Research Kiel, Marine Biogeochemical Modelling, Düsternbrooker Weg 20, 24105 Kiel, Germany

Correspondence to: B. Su (bsu@geomar.de)

Abstract

Local coupling between nitrogen fixation and denitrification in current biogeochemical models could result in a run-away feedback in open-ocean oxygen minimum zones (OMZs), eventually stripping OMZ waters of all fixed nitrogen. This feedback does not seem to operate at full
5 strength in the ocean, as nitrate does not generally become depleted in open-ocean OMZs. To explore in detail possible mechanisms that prevent nitrogen depletion in the OMZ of the Eastern Tropical South Pacific (ETSP), we develop a box model with fully prognostic cycles of carbon, nutrients, and oxygen in the upwelling region and its adjacent open ocean. Ocean circulation is calibrated with $\Delta^{14}C$ data of the ETSP. The sensitivity of the simulated nitrogen cycle to
10 nutrient and oxygen exchange and ventilation from outside the model domain and to remineralization scales inside an OMZ is analysed. For the entire range of model configurations explored, we find that the fixed-N inventory can be stabilized at non-zero levels in the ETSP OMZ only if the remineralization rate via denitrification is slower than that via aerobic respiration. In our optimum model configuration, lateral oxygen supply into the model domain is required at rates
15 sufficient to oxidize at least about one fifth of the export production in the model domain to prevent anoxia in the deep ocean. Under these conditions, our model is in line with the view of phosphate as the ultimate limiting nutrient for phytoplankton, and implies that for the current notion of nitrogen fixation being favored in N-deficit waters, the water column of the ETSP could even be a small net source of nitrate.

20 ## 1 Introduction

The oceanic fixed nitrogen (fixed-N) budget is an essential control on the potential of the ocean to sequester atmospheric CO_2 via the marine biological pump. Denitrification is generally recognized as a major loss of fixed nitrogen, whereas the balance of the global oceanic nitrogen budget remains controversial. Accordingly, estimates derived from both field data and model
25 analyses for the global oceanic fixed-N budget range from sources roughly balancing sinks (Gruber and Sarmiento, 1997; Gruber, 2004; Eugster and Gruber, 2012; DeVries et al., 2013)

2

to a rather large net deficit between 140 and $234\,\mathrm{Tg\,N\,yr^{-1}}$ (Codispoti et al., 2001; Galloway et al., 2004; Codispoti, 2007).

One of the main uncertainties in the global marine nitrogen budget is the extent of nitrogen loss via denitrification and anaerobic ammonium oxidation (anammox) in oxygen minimum zones (OMZs), located in tropical coastal upwelling regions. Coastal upwelling zones are often associated with very high primary production. Subsequent decomposition of sinking organic matter leads to high levels of oxygen consumption in subsurface waters. Under conditions of sluggish circulation, oxygen-poor source waters, or lack of exchange with oxygenated surface waters, OMZs can develop, usually at intermediate depths of about 200–700 m (Bethoux, 1989; Capone and Knapp, 2007). An OMZ is commonly defined as a water body with an O_2 concentration below $20\,\mathrm{\mu mol\,L^{-1}}$ (Paulmier and Ruiz-Pino, 2009). The four major open-ocean OMZs are in the Eastern North Pacific (ENP), the Eastern Tropical South Pacific (ETSP), the Arabian Sea, and the Bay of Bengal. OMZs currently account for only about 8 % of the global ocean area but observations of intense denitrification and anammox in the OMZs indicate that they could be responsible for 30–50 % of the total fixed-N loss (Gruber and Sarmiento, 1997; Codispoti et al., 2001; Dalsgaard et al., 2005; Paulmier and Ruiz-Pino, 2009).

Canfield (2006) used a simple steady-state box model of a coastal OMZ to show that a positive feedback between N_2 fixation and denitrification could strip the OMZ of all fixed nitrogen when N_2 fixation was permitted to restore the nitrate : phosphate ratio to Redfield proportions in the surface ocean. Observed concentrations of fixed-N (nitrate plus nitrite) in OMZ waters, however, typically range from about 15 to $40\,\mathrm{\mu mol\,L^{-1}}$ (Codispoti and Richards, 1976; Codispoti and Packard, 1980; Morrison et al., 1998; Voss et al., 2001). A possible explanation for the relatively high nitrate concentrations even in the suboxic core of open-ocean OMZs could be low levels of nitrogen fixation in the overlying surface waters (Landolfi et al., 2013). However, recent interpretations of observed fixed-N deficits relative to the Redfield equivalent of phosphorus point to high rates of nitrogen fixation closely related to the upwelling of nitrogen-deficit waters along the South American coast (Deutsch et al., 2007). Although alternative explanations for these nutrient patterns have been proposed in models (Mills and Arrigo, 2010), direct measurements have confirmed the occurrence of nitrogen fixation in and above the OMZ of the

3

ETSP (Fernandez et al., 2011). Global biogeochemical models also generally predict substantial rates of N_2 fixation in the nitrate-deficit waters of the upwelling region of the ETSP that, if not compensated by some ad-hoc slow-down of remineralization in suboxic conditions, lead to a complete draw-down of nitrate in the OMZ (Moore and Doney, 2007; Schmittner et al., 2008). The question of how non-zero nitrate concentrations can be maintained in the OMZ thus still awaits a mechanistic answer.

The computational efficiency of box models makes them suitable for sensitivity analyses requiring thousands of model evaluations. In spite of its simplicity, Canfield's (2006) box model is also able to capture the most important first-order interactions among ocean circulation, nitrogen fixation, denitrification, and OMZs. However, Canfield's model was limited in its power to investigate the influence of open ocean nutrients and oxygen conditions on the upwelling region, because its dynamics were restricted to the OMZ, where all biogeochemical tracers were prescribed in the surrounding waters. Based on Canfield's (2006) steady-state formulation with prescribed oxygen and nutrient concentrations at all depths outside the OMZ, we here present a fully prognostic box model of NO_3^-, PO_4^{3-} and O_2 cycles in a coastal upwelling region and an adjacent ocean basin. We employ this model to examine under which conditions the observed situation of an essentially complete drawdown of subsurface oxygen and an incomplete drawdown of nitrate can be reproduced for the case of the ETSP. Sensitivity experiments explore how nutrient exchange and oxygen ventilation from the southern boundary influence the nitrogen budget within the model domain.

By including a prognostic description not only of conditions within the OMZ, but also in the water surrounding it, we aim to represent local as well as spatially-separated feedbacks between the relatively small OMZ and the much larger open-ocean basin. The model describes net primary and export production by ordinary and N_2-fixing phytoplankton, as well as aerobic and anaerobic remineralization. The latter is generally associated with nitrogen loss, commonly attributed to denitrification (Codispoti, 1995). Anammox has recently been reported as another major pathway for fixed-N removal (Kuypers et al., 2005; Hamersley et al., 2007; Molina and Farías, 2009), but the relative contributions of anammox and denitrification are still a matter of debate (Ward et al., 2009; Bulow et al., 2010). In our model, we do not explicitly resolve the

4

different inorganic nitrogen species and pragmatically consider all loss of fixed-N via anaerobic remineralization as denitrification. In Canfield's (2006) model, most of the physical model parameters were constrained by observations from suboxic upwelling zones in the Arabian Sea and the Eastern Tropical North and South Pacific. The physical dynamics of our model system
5   is governed by vertical and horizontal mixing and advection, which are calibrated with Δ^{14}C data of the ETSP from GLODAP (Global Ocean Data Analysis Project, Key et al., 2004).

2   Model description

Figure 1 shows the model structure, consisting of five boxes representing an upwelling region and an adjacent ocean basin. The U box represents the upper upwelling region. The UM box is
10   the underlying OMZ, where suboxia is expected to develop. The S box represents the surface ocean away from the upwelling zone. Below the S box sits the I box, which represents water of intermediate depth and exchanges water with UM. D is the deep box, which represents water deeper than 500 m. When the UM, I, or D boxes become suboxic, denitrification (Denif) will ensue to remineralize the exported organic matter, causing a loss of nitrate (the only form of
15   fixed inorganic nitrogen in our model) .

Prognostic tracers represent NO_3^-, PO_4^{3-}, O_2, ^{14}C and the biomass of ordinary and N_2-fixing phytoplankton, respectively (Table 1). The rate of concentration change of a tracer, X_i, in box i is composed of physical transport, Transport(X_i), and a sources-minus-sinks term, SMS(X_i), which represents the effects of biotic processes, air–sea gas exchange and, in the case of ^{14}C,
20   radioactive decay on the tracer concentration (Eq. 1).

$$\frac{dX_i}{dt} = \frac{\text{Transport}(X_i) + \text{SMS}(X_i)}{V_i} \quad i \in [\text{U, S, UM, I, D}] \tag{1}$$

where U, S, UM, I and D refer to the model boxes defined above and V_i to the corresponding volumes (Fig. 1).

5

2.1 Transport model

Advection represents the large-scale circulation and is indicated in Fig. 1 by wide grey lines. L_U and L_S are the horizontal scales of the upwelling region and the open ocean, and H_U, H_{UM} and H_D refer to the thickness of the respective boxes. The volumes V_i of the boxes are defined in this 2-D model by $V_i = H_i \cdot L_i$. K_{US}, K_{UM} and K_H are the coefficients of mixing between different boxes. A and B represent the deep and shallow large-scale circulation. The upwelling intensity into box U is given by $A + B$. The tracer transport equations for the standard configuration are given in Appendix A (Eqs. A1–A5). All parameters are defined in Tables 2 and 3.

2.2 Biogeochemical model

The ecological model is composed of two phytoplankton types, ordinary phytoplankton, Phy, and nitrogen fixers, NF. The SMS terms for phytoplankton are obtained as the difference between net primary production (NPP) and mortality (M):

$$\text{SMS}(\text{Phy}_i) = (\text{NPP}^{\text{Phy}_i} - \text{M}^{\text{Phy}_i}) \cdot V_i \quad i \in [\text{U, S}] \tag{2}$$

$$\text{SMS}(\text{NF}_i) = (\text{NPP}^{\text{NF}_i} - \text{M}^{\text{NF}_i}) \cdot V_i \quad i \in [\text{U, S}] \tag{3}$$

Growth of ordinary phytoplankton is described by a Liebig-type dependence on the nitrate and phosphate limitation terms (Eq. 4),

$$\text{NPP}^{\text{Phy}_i} = \mu \cdot \min\left(\frac{N_i}{N_i + N_h}, \frac{P_i}{P_i + P_h}\right) \cdot \text{Phy}_i \quad i \in [\text{U, S}] \tag{4}$$

$$\text{NPP}^{\text{NF}_i} = \mu_{\text{NF}} \cdot \frac{P_i}{P_i + P_h} \cdot \text{NF}_i \quad i \in [\text{U, S}] \tag{5}$$

where i is the model box, μ and μ_{NF} are the maximum growth rates of Phy_i and NF_i respectively. N_i and P_i are nitrate and phosphate concentrations, and N_h and P_h are half-saturation concentrations for nitrate and phosphate. Considering possible viral lysis, phytoplankton aggregation,

6

or a feedback between zooplankton grazing and phytoplankton concentration, a quadratic mortality term is adopted for both Phy and NF in all model configurations (Eq. 6).

$$M^{\text{Phy}_i} = M_q \cdot \text{Phy}_i^2 \qquad M^{\text{NF}_i} = M_q \cdot \text{NF}_i^2 \qquad (6)$$

Both Phy and NF require phosphate, whereas nitrate is required in addition to phosphate only by Phy, and NF can fix N_2 as long as PO_4^{3-} is available (Eq. 4, 5). While the ability to utilise organic P has been proposed as an advantage of diazotrophs (Houlton et al., 2008; Ye et al., 2012), ordinary phytoplankton can also use DOP (e.g., Chu, 1946; Cotner, Jr. and Wetzel, 1992) and a clear advantage of diazotrophs over ordinary phytoplankton in the presence of DOP has never been demonstrated. Thus, we treat all available P to phytoplankton operationally as PO_4^{3-} and assume that all organic phosphate is remineralized to PO_4^{3-} directly. N_2 fixers are given a lower maximum growth rate (μ_{NF}, Eq. 5), which is $1/3$ of the maximum growth rate of ordinary phytoplankton (μ), to account for the high cost of nitrogen fixation (La Roche and Breitbarth, 2005). The dependence of NF on iron is not explicitly considered in this model (Mills et al., 2004). Both types use nitrogen and phosphorus in the Redfield ratio of $16:1$ (Redfield et al., 1963).

Sensitivity experiments are also performed with a configuration where nitrogen fixers preferentially use nitrate when available and cover only the residual nitrogen demand via N_2 fixation, denoted as facultative N_2-fixation, but overall results are found to be virtually unchanged (Appendix B).

Dead phytoplankton is immediately remineralized in the surface layer and underlying boxes according to the respective remineralization fraction f_i of box i. Remineralization occurs preferentially via aerobic respiration, with anaerobic remineralization and the associated nitrogen loss setting in only when all O_2 has been consumed by aerobic respiration. Phytoplankton growth and aerobic remineralization together with denitrification and, once all inorganic nitrogen is consumed, remineralization via sulfate reduction define the SMS terms of the nitrogen and

7

phosphorus cycles:

$$\text{SMS}(N_i) = -\text{NPP}^{\text{Phy}_i} \cdot V_i + \text{Rem}_i^N - \text{Denif}_i \tag{7}$$

$$\text{SMS}(P_i) = -\frac{(\text{NPP}^{\text{Phy}_i} + \text{NPP}^{\text{NF}_i}) \cdot V_i}{r_{\text{p}}} + \text{Rem}_i^P \tag{8}$$

where the remineralization (Rem) and denitrification (Denif) terms are defined in Appendix C.

O_2 is set constant in the surface ocean boxes U and S, which are in immediate contact with the atmosphere, but varies as a function of transport and respiration in the UM, I and D boxes. Thus, the aerobic respiration terms (Res_i) are only needed in the interior boxes UM, I and D:

$$\text{SMS}(O_{2i}) = -\text{Res}_i \quad i \in [\text{UM, I, D}] \tag{9}$$

where Res is defined in Appendix C (Eq. C10). Note that aerobic respiration will, in general, also take place in anoxic model boxes, where it utilizes the O_2 transported from adjacent boxes, before anaerobic respiration starts. All model runs are initialized with O_2, NO_3^- and PO_4^{3-} annual data from the World Ocean Atlas 2009 (Garcia et al., 2010a,b), averaged over the regions indicated in Table 4.

2.3 Model calibration

In the present work, the prescribed transport among the different boxes in terms of advection and mixing was calibrated by fitting the modeled $\Delta^{14}C$ distribution to the GLODAP "pre-bomb" $\Delta^{14}C$ distribution of the Eastern Tropical South Pacific (Key et al., 2004; Table 4). The ^{13}C fractionation-corrected ratio of $^{14}C/^{12}C$, $\Delta^{14}C$, is commonly used in ocean modeling to evaluate and calibrate model physics (Toggweiler et al., 1989; Shaffer and Sarmiento, 1995), because it tends to cancel the effect of the biotic downward transport of ^{14}C with the rain of organic particles produced by marine organisms. For practical reasons, we employ the arbitrary scale introduced by Shaffer and Sarmiento (1995) to represent $\Delta^{14}C$, and define $\widehat{\Delta^{14}C}$. $\widehat{\Delta^{14}C}$ can be converted to $\Delta^{14}C$ units as follows:

$$\Delta^{14}C = 1000(\widehat{\Delta^{14}C} - 1)\%_o \tag{10}$$

8

The ^{14}C dynamics in the model includes input from the atmosphere at the sea surface and radioactive decay with decay rate $\lambda = 1.21 \times 10^{-4}\,\mathrm{yr}^{-1}$ within the model domain. The SMS term for $\widehat{\Delta^{14}\mathrm{C}}$ is thus given by:

$$\mathrm{SMS}(\widehat{\Delta^{14}\mathrm{C}_i}) = \left(\frac{g_i(\widehat{\Delta^{14}\mathrm{C}_a} - \widehat{\Delta^{14}\mathrm{C}_i})}{H_i} - \lambda\widehat{\Delta^{14}\mathrm{C}_i}\right) \cdot V_i \quad i \in [\mathrm{U, UM, S, I, D}] \tag{11}$$

where $\widehat{\Delta^{14}\mathrm{C}_i}$ is the value of $\widehat{\Delta^{14}\mathrm{C}}$ in box i, $\widehat{\Delta^{14}\mathrm{C}_a}$ is the atmospheric $\widehat{\Delta^{14}\mathrm{C}}$, and g_i is the gas exchange rate. For $i \in [\mathrm{UM, I, D}]$, $g_i = 0$. We assume that the $\Delta^{14}\mathrm{C}$ of the preindustrial atmosphere, $\Delta^{14}\mathrm{C}_a$, is $0\,‰$. Therefore, $\widehat{\Delta^{14}\mathrm{C}_a}$ is 1. Model configurations with an open southern boundary also include ^{14}C exchange with the adjacent subtropical ocean. We also investigate how sensitive our main conclusions are to the uncertainty in the $\Delta^{14}\mathrm{C}$ data. Table 4 shows the $\Delta^{14}\mathrm{C}$ values used for the calibrations of the different model configurations. Transport and SMS terms for ^{14}C constitute a system of 5 linear equations with 7 parameters, including 5 transport parameters, A, B, K_{US}, K_{UM}, K_{H}, and 2 air–sea ^{14}C exchange coefficients, g_{U} and g_{S}. After setting g_{U} and g_{S}, the 5 equations can be inverted to solve for the transport parameters. A detailed description of the inversion scheme is provided in Appendix D.

2.4 Model configurations

Above transport and biogeochemical formulations define the standard (STD) configuration, where the transport and biogeochemical models are applied without exchange with the southern boundary ("SO" in Fig. 1). Fixed fractions f_i of net primary production in U and S are remineralized in the U, UM, S and I boxes, with the remainder being remineralized in D (Fig. 1). Nutrient regeneration is assumed to be instantaneous.

In order to investigate the relationships between the different biotic and physical processes and the nitrogen cycle in an OMZ, we introduce seven additional model configurations. The main differences to the STD configuration are shown in Table 5. (1) In the Reduced-denitrification (RD) configuration, denitrification in the OMZ is reduced to $1/5$ of the rate of

the STD configuration following the procedure applied in the global biogeochemical circulation model by Schmittner et al. (2008). When oxygen is exhausted in the OMZ, denitrification within the UM box will be responsible for only $1/5$ of the remaining organic matter remineralization and the remainder will be remineralized in the D box (Eqs. C7 and C8). (2) The Ventilation-D (VD) configuration modifies the STD configuration in that the southern boundary of the model domain is partially opened to allow ventilation of O_2 and ^{14}C (but not NO_3^- and PO_4^{3-}) to the D box from the southern subtropical ocean (Eq. A7). The circulation parameters were recalibrated to account for ventilation of ^{14}C from the south. Ventilation is simulated by applying lateral mixing with the subtropical oligotrophic ocean tracer reservoirs with prescribed ^{14}C and O_2 concentrations inferred from observations. All other biogeochemical processes within the model domain are kept the same as in the STD configuration. (3) In the Ventilation-D + Reduced-denitrification (VDRD) configuration, the reduced denitrification rate is applied in the VD configuration. (4) In the Ventilation-ID (VID) configuration, the partially open southern boundary is extended to allow ventilation of O_2 and ^{14}C also into the I box from the subtropical ocean (Eq. A6). Again, circulation parameters are recalibrated against observed $\Delta^{14}C$ taking into account the ^{14}C exchange between the subtropical ocean and the I and D boxes. (5) In the Ventilation-ID + Reduced-denitrification (VIDRD) configuration, the reduced denitrification rate is also applied in the VID configuration. (6) In the Open-boundary (OB) configuration, nutrient mixing is added to the VID configuration to allow for exchange of nutrients between the I and D boxes and the subtropical ocean. (7) In the Open-boundary + Reduced-denitrification (OBRD) configuration, the reduced-denitrification rate is again added to the OB configuration. The physical transports of NO_3^- and PO_4^{3-} for the I and D boxes in the last six configurations are represented by Eqs. (A6) and (A7) in Appendix A.

2.5 Sensitivity experiments

Two sensitivity experiments are performed for each of the VID and OB configurations to explore possibilities for preventing NO_3^- depletion in the OMZ: (a) different reduced remineralisation rates (f_{UM}) and (b) facultative N_2-fixation (see Appendix E).

10

For the OBRD configuration, three sensitivity experiments are performed to investigate our model sensitivity to variable physical transports and biogeochemical tracer concentrations: (1) The mixing rate with the southern boundary, K_H, is reduced for individual tracers (nutrients, oxygen) or combinations thereof from full rates to zero. (2) Simulations are repeated with in-5 dividual circulation parameters varied by $\pm 50\%$ to explore the sensitivity with respect to the circulation parameters of the box model. (3) The sensitivity of NO_3^- and O_2 concentrations in the OMZ to different physical parameters derived from variations of the $\Delta^{14}C$ data and O_2 concentrations in the U-box is also examined.

The literature ranges in Table 3 provide only a rough guide for the biogeochemical parame-10 ters. The sensitivity of r_p, μ, μ_{NF}, N_h and P_h is tested in the OBRD configuration by changing each of them according to the literature range. Effects of changing the remineralisation fractions f_U, f_{UM}, f_S, and f_I are examined by redistributing remineralisation between the U and UM, and S and I boxes. These sensitivity experiments will be discussed in Section 3.3 below.

3   Results

15 The physical circulation parameters calibrated with $\Delta^{14}C$ are given in Table 2. The resulting circulation is comparable with our expectations for the upwelling region of the Eastern Tropical South Pacific. The parameters of the biogeochemical model are shown in Table 3.

3.1   Biogeochemical tracer concentrations

Nutrient and oxygen concentrations in the upwelling region (boxes U and UM) are influenced 20 by physical exchange with regions outside the upwelling zone (boxes I and D) and subsequent remineralization of exported organic matter. The results for biogeochemical tracer concentrations of the STD, RD, VIDRD and OBRD configurations are shown in Fig. 2 and will be used to develop our main conclusions, whereas those of the VD, VDRD, VID and OB configurations are also included in Fig. 3 and described in Appendix E.

11

In the STD configuration, NO_3^- levels in the UM box are quickly exhausted by denitrification in the UM box (black bars in Fig. 2), where decomposition of exported organic matter consumes all O_2 entering the UM box via advection and diffusion, and all NO_3^- entering via physical transport and remineralization of exported organic matter. O_2 is also depleted in the D
5   box, owing to weak ventilation. This results in over 90 % of the initial nitrate being lost from the model domain by denitrification once the model has reached steady state. The large nitrate deficit with respect to phosphate in the upwelling waters results in nitrogen fixers becoming dominant in the U box despite having a lower maximum growth rate than ordinary phytoplankton (black bars in Fig. 2a, c).

10   In the RD configuration, complete NO_3^- exhaustion in the UM box is prevented (grey bars in Fig. 2). There is some observational evidence for the efficiency of decomposition of organic matter driven by denitrification in some high-productivity areas being lower than for respiratory processes in the presence of sufficient dissolved oxygen (Liu and Kaplan, 1984; Devol and Hartnett, 2001; Van Mooy et al., 2002). In our model, this mechanism helps preventing NO_3^-
15   depletion in the OMZ because less nitrate is consumed by denitrification during the passage of the particles through the OMZ. However, the NO_3^- concentration in the UM box is only 3.25 µmol kg^{-1}, far less than the literature range from about 15 to 40 µmol L^{-1}. The additional organic matter now passing through the OMZ must be remineralized in the D box, which still becomes anoxic in this configuration. Even though the RD configuration fails to simulate the
20   realistic biogeochemical tracer concentrations in the OMZ and its adjacent ocean, it reveals a possible mechanism for preventing NO_3^- depletion in the OMZ.

While a reduced remineralisation rate under suboxic conditions appears to be a prerequisite for maintaining non-zero nitrate in the OMZ (Fig. 3), we find that ventilation of O_2 from the lateral subtropical ocean into the model domain is essential for preventing anoxic condition in
25   the D box. But even ventilation of O_2 into both I and D boxes fails to prevent NO_3^- depletion in the UM box in the VID configuration (Fig. 3i). After reducing the denitrification rate in the OMZ, which is the configuration denoted as VIDRD, NO_3^- depletion is prevented (bars with horizontal lines in Fig. 2). Compared to the RD configuration, NO_3^- concentration in the UM box is in a realistic range (15-40 µmol kg^{-1}) for the OMZ, and O_2 concentrations in the I and

12

D boxes are also closer to the WOA2009 data, but still about 15.0% and 22.7% lower than the observations (blue dashed lines in Fig. 2).

In the OBRD configuration, nutrients are exchanged in addition to O_2 between the subtropical ocean and the I and D boxes, together with reducing the denitrification rate under suboxic conditions. N_{UM} depletion is prevented and N_{UM} approaches a concentration of $20\,\mu mol\,kg^{-1}$ at steady state (bars with horizontal lines in Fig. 2). The UM box is suboxic and the O_2 concentrations in the I and D boxes agree very well with the WOA2009 data (blue dashed lines in Fig. 2). Overall, tracer distributions simulated by the OBRD configuration agree best with the observations. In the sensitivity configuration OB, where only nutrients are exchanged in addition to O_2 between the subtropical ocean and the I and D boxes, nitrate is still exhausted in the OMZ (Fig. 3m).

3.2 Biogeochemical fluxes

For the biogeochemical fluxes, we focus on the STD, RD, VIDRD and OBRD configurations (configurations in bold in Table 5), since they show most clearly the mechanisms responsible for preventing NO_3^- depletion in the OMZ (Fig. 4). Denitrification rates are much higher in the STD than in the RD configuration (black and grey bars in Fig. 4 respectively), even though the physical parameters are the same in the two configurations, leading to nitrate exhaustion in the UM box of the STD but not in the RD configuration. In both VIDRD and OBRD configurations, NO_3^- depletion is prevented (bars with horizontal and vertical lines in Fig. 2e). Denitrification is weaker in the OBRD than in the VIDRD configuration (bars with horizontal lines in Fig. 4), even though the physical parameters are the same in both, keeping more NO_3^- in the UM-box in the OBRD configuration. Aerobic respiration in the UM box continues even when the UM box is anoxic. It consumes all O_2 entering the UM box via the various physical transport processes and thereby oxidizes about 8.7 %, 64 %, 85 % and 92 % of the organic matter remineralized (denitrification+ aerobic respiration) in the UM box in all four configurations, STD, RD, VIDRD and OBRD, respectively. Aerobic respiration is increased in the OBRD configuration compared with the VIDRD configuration (92 % vs. 85 %) at the expense of denitrification.

13

Compared with the VIDRD configuration, total PO_4^{3-} in the model domain decreases by about 28 % in the OBRD configuration at steady state, and the net PO_4^{3-} flux out of the I box and the corresponding net flux of PO_4^{3-} from the subtropical ocean into the D box causes a 9.6 % decrease in organic matter exported into the UM box. This explains why NO_3^- concentrations in the OMZ and O_2 concentrations in the I and D boxes are slightly higher (bars with vertical lines in Fig. 2). Restricting, in a hypothetical sensitivity experiment, exchange with the subtropical oligotrophic ocean to NO_3^- and O_2 does not result in higher O_2 concentrations in the I and D boxes, because PO_4^{3-} is conserved and export production dose not change substantially. Restricting, on the other hand, exchange to PO_4^{3-} and O_2 depresses production and organic matter decomposition by almost the same amount as in the model run that exchanges NO_3^-, PO_4^{3-} and O_2, and succeeds in driving O_{2I} and O_{2D} concentrations closer to the observations (not shown). Thus, opening the model boundary to PO_4^{3-} and O_2 helps to improve the model results with respect to those of the VIDRD configuration that does not exchange PO_4^{3-} across the southern boundary.

3.3 Model sensitivity

In sensitivity experiments of the OBRD configurations, designed to elucidate the importance of the influence of the subtropical ocean on the model domain, we reduce the mixing rates (K_H) of O_2, NO_3^- and PO_4^{3-} across the southern boundary in different combinations (two of them are shown in Fig. 5). Total net primary production (NPP) is the same when varying the mixing rate of either only O_2 or O_2 together with NO_3^-, as long as the PO_4^{3-} exchange rate with the subtropical ocean remains unchanged (dotted lines in Fig. 5b). The reason is that changes in nitrate exchange with the subtropical ocean are compensated by changes in denitrification and nitrogen fixation. This implies that NPP is, at steady state, determined only by phosphate availability. Once the total NPP of NF and Phy is determined by PO_4^{3-} supply, aerobic respiration will increase with increasing O_2 supply, while anaerobic remineralization will decrease (solid and dashed lines in Fig. 5c). Comparing simulations that vary the mixing rate of O_2 together with that of PO_4^{3-}, with simulations that vary the mixing rate of O_2 together with that of NO_3^- and PO_4^{3-} (dotted lines in Fig. 5g) reveals that the combined NPP of Phy and NF decreases with

14

decreasing PO_4^{3-} inventory at low mixing rates and increases with increasing PO_4^{3-} inventory at high mixing rates, irrespective of NO_3^- mixing rate.

It turns out that NO_3^- depletion in the OMZ is prevented in the four sensitivity experiments of Fig. 5 no matter how much O_2 is supplied from the subtropical ocean into the model domain. But anoxia in the D box can only be prevented if the external O_2 supply can oxidise more than about 20 % export production in the model domain (solid lines in Fig. 5e, j). This ratio can vary according to the size of S box. It increases for a smaller S box, because a smaller S box leads to less downward O_2 supply from the surface box into the lower model domain and more lateral ventilation is needed, and vice versa (not shown). These experiments also reveal an interesting link among the O_2 supply from the subtropical ocean, the nitrate concentration in the OMZ, and the NO_3^- flux between the model domain and surrounding ocean. As soon as the O_2 supply from the subtropical ocean accounts for about 17.5 % of the respiratory O_2 consumption, the model domain turns into a small net source of NO_3^- (dashed lines in the first row of Fig. 5). Once anoxia is prevented in the D box, the nitrate concentration in the OMZ (UM box) increases quite strongly from about $15\,\mu mol\,kg^{-1}$ to reach about $20\,\mu mol\,kg^{-1}$ at full mixing strength.

The conclusion that the model domain is a small pelagic net NO_3^- source in the OBRD configuration does not change when individual physical transport parameters vary by up to $\pm 50\%$ (Fig. 6). Varying biogeochemical parameters also does not affect this conclusion. The finding that the model domain is a net NO_3^- source is also tenable for all suites of physical transport parameters in the literature range for which the D-box is oxic (Fig. 7).

The oxygen concentrations in the I and D boxes increase in sensitivity model runs with physical parameters calibrated from increased ^{14}C concentrations (lower water mass age, figure not shown). NO_3^- depletion is prevented in the OMZ in the OBRD configuration within the range of about $\pm 10\,\%$ around the default ventilation intensity (Fig. 8a). The UM box remains anoxic when $\Delta^{14}C$ is varied within this range, which indicates that this mechanism for preventing NO_3^- depletion in the OMZ may be robust against modest changes in the regional ocean circulation patterns. Meanwhile, NO_3^- and O_2 in the UM box are quite insensitive to the O_2 concentration in the U-box for this configuration (Fig. 8b).

15

Varying biogeochemical parameters affects individual model predictions but not our main conclusions. The strongest effects are those of varying the N:P ratio r_p and the remineralisation fractions (f_U, f_{UM}, f_S, and f_I) (Fig. 6). Lowering r_p to 12 increases N_{UM} by about 35 %, but cannot change the strength of our model domain as a net NO_3^- source. Increasing r_p to 20

5　decreases N_{UM} by about 18 %, but triples the strength of our model domain as a NO_3^- source. However, observations indicate that r_p for the ETSP is more likely to be higher than lower compared to the Redfield N:P ratio of 16 (Franz et al., 2012). Increasing the maximum growth rate of NF, μ_{NF}, to $1/2\mu$, the maximum growth rate of Phy, results in higher N_{UM} concentrations and our model domain being a larger NO_3^- source. Intuitively, decreasing μ_{NF} to $1/4\mu$ results

10　in lower N_{UM} concentrations and our model domain becoming a smaller NO_3^- source. Varying the NO_3^- half saturation constant, N_h, results in virtually unchanged results. N_{UM} increases when changing remineralisation fractions in the intermediate boxes (f_{UM} and f_I) from 70 % to 50 % and 30 % respectively, effectively lowering export production via lowering the export ratio. Nevertheless the qualitative behaviour of the model remains the same in these sensitivity

15　experiments.

4　Discussion and conclusions

Nitrogen is often considered to be the primary limiting nutrient in marine upwelling regions with OMZs (Cline and Richards, 1972; Codispoti and Christensen, 1985; Morrison et al., 1998; Voss et al., 2001), where denitrification rates can be high and are generally thought to cause

20　a major loss of NO_3^- from the world ocean. The nitrogen deficit is commonly assumed to stimulate N_2 fixation, both in observational estimates of N_2 fixation (Deutsch et al., 2007; Monteiro et al., 2010) and in current descriptions of N_2 fixation in biogeochemical models (Moore and Doney, 2007; Schmittner et al., 2008). However, if N_2 fixation is tightly linked to nitrogen loss processes, denitrification of organic matter derived from N_2 fixation can consume more nitro-

25　gen than was fixed via N_2 fixation and thereby lead to a vicious cycle of run-away nitrogen loss (Landolfi et al., 2013). This has been found to lead to total depletion of NO_3^- in the OMZ of box models (Canfield, 2006) and global biogeochemical circulation models (Moore and Doney,

16

2007; Schmittner et al., 2008). For our fully prognostic 5-box model, we have identified the mechanisms capable of arresting the run-away nitrogen loss that can result from a close coupling of nitrogen fixation and denitrification (Landolfi et al., 2013) and maintaining realistic non-zero NO_3^- concentrations in open-ocean OMZs of the ETSP: reduced NO_3^- consumption by denitrification owing to slower remineralization under suboxic compared to oxic conditions, coupled with lateral ventilation of oxygen and, to some extent, nutrients with the subtropics.

In this work, the model configuration with reduced denitrification rate and lateral ventilation and nutrient exchange (OBRD configuration) performs best with respect to the observations, whereas reduced rates of denitrification alone lead to unrealistic O_2 depletion in the deep waters, and reduced rates of denitrification combined with only O_2 ventilation in the D or both I and D boxes still underestimate the WOA2009 data for O_2 in the I and D boxes. By allowing for exchange of O_2 and nutrients with the subtropical ocean in the OBRD configuration, the delicate balance between sufficient O_2 supply required for maintaining high levels of aerobic respiration and sufficient PO_4^{3-} loss through the open boundary appears fulfilled. Compared with other box models (Shaffer and Sarmiento, 1995; Tyrrell, 1999; Deutsch et al., 2004; Canfield, 2006; Mills and Arrigo, 2010; Eugster and Gruber, 2012; DeVries et al., 2012), the box model we use here explicitly employs both a reduced-denitrification rate and an open boundary condition, which seems to be a prerequisite for the ability to simulate realistic nitrate conditions in the OMZ and oxygen concentrations in the adjacent ocean.

The NO_3^- loss by denitrification in the OMZ of the OBRD configuration is compared with that of other model-based and observational estimates in Table 6. Our simulated denitrification is consistent with the results of Somes et al. (2010) and DeVries et al. (2013) for the ETSP, lower than the estimate of Bianchi et al. (2012) and Kalvelage et al. (2013), but higher than that of Mills and Arrigo (2010). However, the estimated denitrification by Bianchi et al. (2012) represents that of the entire South Pacific but not only the ETSP. The Kalvelage et al. (2013) model has much higher fixed-N influx into the OMZ via physical transport than our model, which could compensate for their more intense NO_3^- loss by denitrification.

Phosphate turns out as the ultimate limiting nutrient in our model (Fig. 5), and hence determines the nitrogen content of the OMZ. This strong control of the N cycle by phosphate is

similar to the finding of previous models (e.g. Lenton and Watson, 2000; Canfield, 2006), where the occurrence and extent of oceanic anoxia was also tightly linked to phosphate supply. These studies explicitly assumed that N_2 fixation acts to restore surface-oceanic dissolved inorganic N : P ratio towards the Redfield ratio. By contrast, we do not prescribe the effect of nitrogen fixation on surface inorganic nutrients, and the finding of phosphate as the ultimate limiting nutrient is obtained regardless of whether NF responds directly to the N : P ratio in the surface ocean or whether NF is inhibited by the presence of NO_3^- (see Appendix B).

Even though our model indicates only a weak dependence of simulated NO_3^- concentrations in the OMZ on the lateral O_2 supply from the subtropical ocean, O_2 depletion in the adjacent ocean can be prevented only when the O_2 supply from the subtropical ocean accounts for more than 20 % of the O_2 required to oxidize export production from the surface ocean of our model domain (U and S boxes). This value only varies between about 17 % and 23 %, when the size of the S box varies by ± 50 %, indicating that our above conclusion is rather insensitive to our choice for the model domain. The O_2 supply from the subtropical ocean might be also linked to the balance of the regional fixed-N cycle. In the most realistic (OBRD) configuration, the balance of water-column denitrification and nitrogen fixation is tightly linked to the nitrate concentration in the OMZ: if the model domain acts as a sink for NO_3^-, nitrate concentrations in the OMZ do not exceed about 15 μmol kg^{-1}, i.e., the lower limit of current observations, 15 to 40 μmol kg^{-1} (Codispoti and Richards, 1976; Codispoti and Packard, 1980; Morrison et al., 1998; Voss et al., 2001). Nitrate concentrations close to those commonly found in OMZs are predicted only when nitrogen fixation exceeds water-column denitrification and the ocean basin containing the OMZ becomes a net source of NO_3^- (Fig. 5a, f).

There are no specific data or model results focusing on the water-column nitrogen balance of the ETSP. Our simulations using a parameterisation where nitrogen fixation is inhibited by the presence of nitrate yield very similar results, only with slightly reduced nitrogen fixation resulting in a somewhat reduced (by ≤ 15 %) nitrogen source for strong enough lateral oxygen supply. Ganachaud and Wunsch (2002) estimated a net northward NO_3 transport of 270 ± 170 kmol s^{-1} (119.2 $\pm$ 75.1 Tg N yr^{-1}) across 17° S into the ETSP in a geostrophic inverse box model, which indicates that the ETSP is a net nitrogen sink, but their estimate included

benthic denitrification, which is not accounted for in our current analysis. In a model-guided analysis, DeVries et al. (2012) predicted water-column denitrification rates of 21–33 $\mathrm{Tg\,N\,yr^{-1}}$ by simulating the distribution of observed dissolved N_2 gas produced by denitrifying bacteria. From an ocean circulation-biogeochemical model-based analysis of nutrient concentrations and transport rates, Deutsch et al. (2007) estimated nitrogen fixation rates in the Pacific Ocean of about 95 $\mathrm{Tg\,N\,yr^{-1}}$, half of which was speculated to occur in the ETSP. From these estimates, we cannot rule out that the water column of the ETSP is a net source of NO_3^-, which would be consistent with our results obtained in the OBRD configuration. More recently, Eugster and Gruber (2012) probabilistically estimated nitrogen fixation and water-column and benthic denitrification separately in their box model, which appears to be consistent with our results as their results also indicate that the water column of the IndoPacific is a large fixed-N source.

Based on our model results, we conclude that reduced NO_3^- consumption by denitrification owing to slower remineralization under suboxic conditions together with lateral transport is essential to arrest the vicious cycle of run-away fixed-N loss in the OMZ. More research is needed to better constrain the model parameters, in particular the upwelling transport and the difference between the organic matter remineralisation rate via aerobic respiration and anaerobic denitrification.

Appendix A

Physical transports of a tracer X among the boxes U, UM, S, I, and D are defined for the STD configuration as follows:

$$\text{Transport}(X_U) = (X_{UM} - X_U)(A + B + K_{US}) \cdot L_U \tag{A1}$$

$$\text{Transport}(X_{UM}) = [AX_D + BX_I - X_{UM}(A + B) + K_{US}(X_U - X_{UM})] \cdot L_U$$
$$+ K_{UM}(X_D - X_{UM}) \cdot L_U + K_H(X_I - X_{UM}) \cdot H_{UM} \tag{A2}$$

$$\text{Transport}(X_S) = (A + B)(X_U - X_S) \cdot L_U + K_{US}(X_I - X_S) \cdot L_S \tag{A3}$$

$$\text{Transport}(X_{\text{I}}) = (A + B)(X_{\text{S}} - X_{\text{I}}) \cdot L_{\text{U}} + K_{\text{H}}(X_{\text{UM}} - X_{\text{I}}) \cdot H_{\text{UM}}$$
$$+ K_{\text{US}}(X_{\text{S}} - X_{\text{I}}) \cdot L_{\text{S}} + K_{\text{UM}}(X_{\text{D}} - X_{\text{I}}) \cdot L_{\text{S}} \tag{A4}$$

$$\text{Transport}(X_{\text{D}}) = A\,(X_{\text{I}} - X_{\text{D}}) \cdot L_{\text{U}} + K_{\text{UM}}(X_{\text{UM}} - X_{\text{D}}) \cdot L_{\text{U}} + K_{\text{UM}}(X_{\text{I}} - X_{\text{D}}) \cdot L_{\text{S}} \tag{A5}$$

5 For the VD, VDRD, VID, VIDRD, OB and OBRD configurations, Eqs. (A4) and (A5) are modified to read:

$$\text{Transport}(X_{\text{I}}) = (A + B)(X_{\text{S}} - X_{\text{I}}) \cdot L_{\text{U}} + K_{\text{H}}(X_{\text{UM}} - X_{\text{I}}) \cdot H_{\text{UM}}$$
$$+ K_{\text{US}}(X_{\text{S}} - X_{\text{I}}) \cdot L_{\text{S}} + K_{\text{UM}}(X_{\text{D}} - X_{\text{I}}) \cdot L_{\text{S}}$$
$$+ K_{\text{H}}(X_{\text{SI}} - X_{\text{I}}) \cdot H_{\text{UM}} \tag{A6}$$

$$\text{Transport}(X_{\text{D}}) = A\,(X_{\text{I}} - X_{\text{D}}) \cdot L_{\text{U}} + K_{\text{UM}}(X_{\text{UM}} - X_{\text{D}}) \cdot L_{\text{U}} + K_{\text{UM}}(X_{\text{I}} - X_{\text{D}}) \cdot L_{\text{S}}$$
$$+ K_{\text{H}}(X_{\text{SD}} - X_{\text{D}}) \cdot H_{\text{D}} \tag{A7}$$

15 The transport equations (Eqs. A1 and A3) are modified for Phy and NF because Phy and NF are assumed to be capable of regulating their buoyancy and exist only in U and S without being transported vertically between the U and UM or the S and I boxes.

Appendix B

20 It is well known from laboratory studies that diazotrophic phytoplankton can also utilize nitrate for growth, denoted as facultative N_2-fixation (e.g., Holl and Montoya, 2005). Schmittner et al. (2008) introduced a formulation where nitrogen fixers preferentially use nitrate when available and cover only the residual nitrogen demand via N_2 fixation. In order to examine the behavior of our model when nitrogen fixers (NF) preferentially use nitrate, nitrogen fixation is separated

20

from diazotroph growth, as in Schmittner et al. (2008):

$$\text{Nitrogen-fixation}_i = \left(1 - \frac{N}{N + N_h}\right) \cdot \text{NPP}^{\text{NF}_i} \qquad i \in [U, S] \tag{B1}$$

and Eq. (7) was modified to accomodate the additional nitrate uptake by NF as follows:

$$\text{SMS}(N_i) = \left(-\text{NPP}^{\text{Phy}_i} - \left(\text{NPP}^{\text{NF}_i} - \text{Nitrogen-fixation}_i\right)\right) \cdot V_i + \text{Rem}_i^N - \text{Denif}_i$$
$$i \in [U, UM, S, I, D] \tag{B2}$$

After incorporating Eqs. B1 and B2 in our all configurations described in Section 2.2, they behave very similarly compared to Fig. 2, except that Phy_U and Phy_S concentrations are some-

what lower because nitrogen fixers take up NO_3^- as well. Thus, we conclude that our results are robust with respect to assumptions about facultative N_2-fixation by diazotrophs.

Appendix C

The nitrogen cycle in this model includes nitrogen fixation, denitrification, inorganic nitrogen

regeneration by remineralization, physical transport of NO_3^-, and transport of Phy and NF between the U and S boxes. The physical transport process of NO_3^- is the same as for other tracers. Rem_i^N represents nitrogen remineralization in box i with fixed fractions f_i of the net primary production in the overlaying surface boxes.

$$\text{Rem}_U^N = f_U M(\text{Phy}_U + \text{NF}_U) \cdot H_U \cdot L_U \tag{C1}$$

$$\text{Rem}_{UM}^N = f_{UM} M(\text{Phy}_U + \text{NF}_U) \cdot H_U \cdot L_U \tag{C2}$$

$$\text{Rem}_S^N = f_S M(\text{Phy}_S + \text{NF}_S) \cdot H_U \cdot L_S \tag{C3}$$

$$\text{Rem}_I^N = f_I M(\text{Phy}_S + \text{NF}_S) \cdot H_U \cdot L_S \tag{C4}$$

$$\text{Rem}_D^N = M\big[(1 - f_U - f_{UM})(\text{Phy}_U + \text{NF}_U) \cdot L_U \\ + (1 - f_S - f_I)(\text{Phy}_S + \text{NF}_S) \cdot L_S\big] \cdot H_U \tag{C5}$$

Denitrification (Denif) is the nitrogen loss to N_2 when UM, I and D are anoxic. It is defined as:

$$\text{Denif}_i = \max(\text{Rem}_i^N - \frac{\text{Res}_i}{r_a}, 0) \cdot \frac{r_c}{r_{den}} \quad i \in [\text{UM, I, D}] \tag{C6}$$

with the aerobic respiration term Res_i given below (Eq. C10). In the RD, VDRD, VIDRD and OBRD configuration, the equations for denitrification in the i box and remineralization in D are given by:

$$\text{Denif}_i = \frac{1}{5} \cdot \max(\text{Rem}_i^N - \frac{\text{Res}_i}{r_a}, 0) \cdot \frac{r_c}{r_{den}} \quad i \in [\text{UM, I}] \tag{C7}$$

$$\text{Rem}_D^N = M\big[(1 - f_U - f_{UM})(\text{Phy}_U + \text{NF}_U) \cdot L_U + (1 - f_S - f_I)(\text{Phy}_S + \text{NF}_S) \cdot L_S\big] \cdot H_U \\ + 4 \cdot \frac{\text{Denif}_i \cdot r_{den}}{r_c} \quad i \in [\text{UM, I}] \tag{C8}$$

All the organic matter is composed according to the Redfield Ratio, i.e., $C : N : P = 106 : 16 : 1$. Rem_i^P represents phosphate remineralization in box i, which is obtained by dividing Rem_i^N by the Redfield $N : P$ ratio, r_p:

$$\text{Rem}_i^P = \frac{\text{Rem}_i^N}{r_p} \quad i \in [\text{U, S, UM, I, D}] \tag{C9}$$

Respiration (Res_i) is considered in the intermediate and deep ocean. In the presence of sufficient oxygen or when oceanic circulation supplies enough O_2, organic matter will be preferentially oxidized by respiration. We use a ratio of $-O_2 : N = 170 : 16$ during oxic remineralization of organic matter (Anderson and Sarmiento, 1994).

$$\text{Res}_i = \begin{cases} r_a \cdot \text{Rem}_i^N & \text{if} \quad O_{2i} > 0 \\ \min\big(\text{Transport}(O_{2i}), r_a \cdot \text{Rem}_i^N\big) & \text{if} \quad O_{2i} = 0 \end{cases} \quad i \in [\text{UM, I, D}] \tag{C10}$$

Appendix D

Transport and SMS terms for $\widehat{^{14}C}$ constitute a system of 5 linear equations including transport parameters A, B, K_{US}, K_{UM} and K_H, which are inverted from the $\Delta^{14}C$ values with air–sea

5 $\Delta^{14}C$ exchange rates g_U and g_S for the U and S boxes respectively as inputs. All possible combinations of values (with a step size of $0.01\ \mathrm{m\,yr^{-1}}$) for g_U and g_S are applied to derive the values for transport parameters A, B, K_{US}, K_{UM} and K_H. g_U and g_S are constrained in a two-step procedure. First, all combinations are determined which result in transport parameters in the literature range in Table 3. Finally, the combination giving the most realistic biogeochemi-

10 cal tracer concentrations (closest to observations) is chosen for the experiments in the main text (Fig. 3). This approach for determining the physical transport parameters is applied to obtain the ones in Table 2.

Appendix E

15 The VD, VDRD, VID and OB configurations are sensitivity configurations that we employ to explore the ability of several mechanisms for preventing nitrogen exhaustion in the OMZ. Even though all of them fail in simulating realistic biogeochemical tracer concentrations compared with observations, they reveal insights into the effects of the respective mechanisms.

The VD configuration, which differs from the STD configuration in supplying additional O_2

20 from the subtropical ocean into the D box, avoids anoxic deep waters, but fails to prevent nitrate exhaustion in the UM box (Fig. 3e, f). The I and D boxes are oxic at steady state, but NO_3^- is still exhausted by denitrification in the UM box. Comparing the oxygen concentrations of the RD and VD configurations, we conclude that ventilation helps to prevent oxygen depletion in

23

the D box, but this mechanism alone cannot prevent eventual run-away denitrification in the UM box.

After incorporating reduced denitrification in the VDRD configuration, nitrate depletion is prevented and the I and D boxes are oxic (Fig. 3g, h). But the O_2 concentration in the I box is about 28 % lower than that of the WOA2009 data, which indicates that O_2 supply into the D-box only may not suffice to ventilate the model domain.

The VID configuration, which is modified from the VD configuration by including O_2 ventilation into the I box, fails in preventing NO_3^- depletion by denitrification in the OMZ (Fig. 3i, j).

In the OB configuration, nutrients are exchanged in addition to O_2 between the subtropical ocean and the I and D boxes. In this configuration, nitrate exhaustion in the OMZ is still not prevented, even though phytoplankton and nitrogen fixer concentrations are lower in the surface U and S boxes (Fig. 3m, n).

Two further sensitivity experiments were performed for each of the VID and OB configurations to explore how NO_3^- depletion in the UM box can be prevented. (1) Decreasing the fraction of export production remineralized in the UM box (f_{UM}) from 70 % to 56 % makes NO_3^- persist in the UM box. Together with the 20 % remineralization in the U box, this implies that 76 % of the export production is remineralized in the upper 500 m of the ocean. However, the resulting NO_3^- concentration in the UM box is far below the literature range of about 15 to 40 μmol L^{-1}. (2) Facultative N_2-fixation inhibits nitrogen fixation in an environment with high NO_3^- concentrations, but fails to prevent NO_3^- depletion in the UM box.

The sensitivity with respect to the biogeochemical parameters (Section 2.5) is examined for all configurations. We only discuss the sensitivity of the OBRD configuration in Section 3.3, since the sensitivity experiments in all model configurations do not arrest our main conclusion that fixed-N inventory can be stabilized at non-zero levels in the ETSP OMZ only if the remineralization rate via denitrification is slower than that via aerobic respiration. The model behaviour is very similar in all sensitivity experiments, with two exceptions. When μ_{NF} is raised to $1/2\mu$ and remineralization fractions in different boxes are rearranged to $f_U=f_S=60\%$ com-

24

bined with $f_{UM}=f_I=30\%$, the VDRD and VIDRD configurations reach a steady state only in combination with facultative N_2-fixation.

References

Anderson, L. A. and Sarmiento, J. L.: Redfield ratios of remineralization determined by nutrient data analysis, Global Biogeochem. Cy., 8, 65–80, doi:10.1029/93GB03318, 1994.

Bethoux, J. P.: Oxygen consumption, new production, vertical advection and environmental evolution in the Mediterranean Sea, Deep-Sea Res., 36, 769–781, doi:10.1016/0198-0149(89)90150-7, 1989.

Bianchi, D, Dunne, J. P., Sarmiento, J. L. and Galbraith, E. D.: Data-based estimates of suboxia, denitrification, and N_2O production in the ocean and their sensitivities to dissolved O_2, Global Biogeochem. Cy., 26, 1–13, doi:10.1029/2011GB004209, 2012.

Breitbarth, E, Oschlies, A. and LaRoche, J.: Physiological constrains on the global distribution of *Trichodesmium*-effect of temperature on diazotropy, Biogeosciences, 4, 53–61, doi:10.5194/bg-4-53-2007, 2007.

Bulow, S. E., Rich, J. J., Naik, H. S., Pratihary, A. K., and Ward, B. B.: Denitrification exceeds anammox as a nitrogen loss pathway in the Arabian Sea oxygen minimum zone, Deep-Sea Res. Pt. I, 57, 384–393, doi:10.1016/j.dsr.2009.10.014, 2010.

Canfield, D.: Models of oxic respiration, denitrification and sulfate reduction in zones of coastal upwelling, Geochim. Cosmochim. Ac., 70, 5753–5765, doi:10.1016/j.gca.2006.07.023, 2006.

Capone, D. G. and Knapp, A. N.: A marine nitrogen cycle fix?, Nature, 445, 159–160, doi:10.1038/445159a, 2007.

Capone, D. G., Zehr, J. P., Paerl, H. W., Bergman, B., and Carpenter, E. J.: *Trichodesmium*, a globally significant marine cyanobacterium, Science, 276, 1221–1229, doi:10.1126/science.276.5316.1221, 1997.

Caron, D. A. and Dennett, M. R.: Phytoplankton growth and mortality during the 1995 Northeast Monsoon and Spring Intermonsoon in the Arabian Sea, Deep-Sea Res. Pt. II, 46, 1665–1690, doi:10.1016/S0967-0645(99)00039-9, 1999.

Chu. S. P.: The utilization of organic phosphorus by phytoplankton, J. Mar. Biol. Assoc. U. K., 26, 285–295, 1946.

Cline, J. D. and Richards, F. A.: Oxygen deficient conditions and nitrate reduction in the Eastern Tropical North Pacific Ocean, Limnol. Oceanogr., 17, 885–900, 1972.

Codispoti, L. A.: Is the ocean losing nitrate?, Nature, 376, 724, doi:10.1038/376724a0, 1995.

Codispoti, L. A.: An oceanic fixed nitrogen sink exceeding $400 \, \mathrm{Tg \, N \, a^{-1}}$ vs the concept of homeostasis in the fixed-nitrogen inventory, Biogeosciences, 4, 233–253, doi:10.5194/bg-4-233-2007, 2007.

Codispoti, L. A. and Christensen, J.: Nitrification, denitrification and nitrous oxide cycling in the Eastern Tropical South Pacific Ocean, Mar. Chem., 16, 277–300, doi:10.1016/0304-4203(85)90051-9, 1985.

Codispoti, L. A. and Packard, T.: Denitrification rates in the eastern tropical South Pacific, J. Mar. Res., 38, 453–477, 1980.

Codispoti, L. A. and Richards, F.: An analysis of the horizontal regime of denitrification in the eastern tropical North Pacific, Limnol. Oceanogr., 21, 379–388, 1976.

Codispoti, L. A., Brandes, J., Christensen, J., Devol, A., Naqvi, S., Paerl, H., and Yoshinari, T.: The oceanic fixed nitrogen and nitrous oxide budgets: moving targets as we enter the anthropocene?, Sci. Mar., 65, doi:10.3989/scimar.2001.65s285, 2001.

Cotner, Jr.,J. B. and Wetzel., R. G.: Uptake of dissolved inorganic and organic bphosphorus compounds by phytoplankton and bacterioplankton, Limnol. Oceanogr., 37, 232–243, doi:10.4319/lo.1992.37.2.0232, 1992.

Dalsgaard, T., Thamdrup, B., and Canfield, D. E.: Anaerobic ammonium oxidation (anammox) in the marine environment, Res. Microbiol., 156, 457–464, doi:10.1016/j.resmic.2005.01.011, 2005.

Deutsch, C., Sigman, D. M., Thunell, R. C., Meckler, A. N., and Haug, G. H.: Isotopic constraints on glacial/interglacial changes in the oceanic nitrogen budget, Global Biogeochem. Cy., 18, doi:10.1029/2003GB002189, 2004.

Deutsch, C., Sarmiento, J. L., Sigman, D. M., Gruber, N., and Dunne, J. P. Spatial coupling of nitrogen inputs and losses in the ocean, Nature, 445, 163–167, doi:10.1038/nature05392, 2007.

DeVries, T., Deutsch, C., Primeau, F., Chang, B., and Devol, A.: Global rates of water-column denitrification derived from nitrogen gas measurements, Nature, 5, 547–550, doi:10.1038/NGEO1515, 2012.

DeVries, T., Deutsch, C, Rafter, P, A and Primeau.,F:Marine denitrification rates determined from a global 3-d inverse model, *Biogeosciences*, 10, 2481–2496, doi:10.5194/bg-10-2481-2013, 2013.

26

Devol, A. H. and Hartnett., H. E.: Role of the oxygen-deficient zone in transfer of organic carbon to the deep ocean, Limnol. Oceanogr., 46, 1684–1690, doi:10.4319/lo.2001.46.7.1684, 2001.

Eppley, R. W., Rogers, J. N., and McCarthy, J. J.: Half-saturation constants for uptake of nitrate and ammonium by marine phytoplankton, Limnol. Oceanogr., 14, 912–920, doi:10.4319/lo.1969.14.6.0912, 1969.

Eugster, O. and Gruber, N.: A probabilistic estimate of global marine N-fixation and denitrification, Global Biogeochem. Cy., 26, 1–15, doi:10.1029/2012GB004300, 2012.

Franz, J. M. S., Hauss, H., Sommer, U., Dittmar, T., and Riebesell, U.: Production, partitioning and stoichiometry of organic matter under variable nutrient supply during mesocosm experiments in the tropical Pacific and Atlantic Ocean, Biogeosciences, 9, 4629–4643, doi:10.5194/bg-9-4629-2012, 2012.

Fernandez, C., Farías, L., and Ulloa, O.: Nitrogen fixation in denitrified marine waters, PLoS ONE, 6, e20539, doi:10.1371/journal.pone.0020539, 2011.

Furnas, M. J.: In situ growth rates of marine phytoplankton: approaches to measurement, community and species growth rates, J. Plankton Res., 12, 1117–1151, doi:10.1093/plankt/12.6.1117, 1990.

Galloway, J. N., Dentener, F. J., Capone, D. G., Boyer, E. W., Howarth, R. W., Seitzinger, S. P., Asner, G. P., Cleveland, C. C., Green, P. A., Holland, E. A., Karl, D. M., Michaels, A. F. Porter, J. H., Townsend, A. R., and Vörösmarty, C. J.: Nitrogen cycles: past, present and future, Biogeochemistry, 70, 153–226, doi:10.1007/s10533-004-0370-0, 2004.

Ganachaud, A. and Wunsch, C.: Oceanic nutrients and oxygen transports and bounds on export production during the World Ocean Circulation Experiment, Global Biogeochem. Cy., 16, 1–14, doi:10.1029/2000GB001333, 2002.

Garcia, H. E., Locarnini, R. A., Boyer, T. P., Antonov, J. I., Baranova, O. K., Zweng, M. M., and Johnson, D. R.: Volume 3: dissolved oxygen, apparent oxygen utilization, and oxygen saturation, in: World Ocean Atlas 2009, edited by: Levitus, S., NOAA Atlas NESDIS 70, US Government Printing Office, Washington, D. C., p. 344, 2010a.

Garcia, H. E., Locarnini, R. A., Boyer, T. P., Antonov, J. I., Zweng, M. M., Baranova, O. K., and Johnson, D. R.: Volume 4: nutrients (phosphate, nitrate, silicate), in: World Ocean Atlas 2009, NOAA Atlas NESDIS 71, US Government Printing Office, Washington, D. C., p. 398, 2010b.

Gruber, N.: The dynamics of the marine nitrogen cycle and its influence on atmospheric CO_2 variations, in: The Ocean Carbon Cycle and Climate, edited by: Follows, M. and Oguz, T., vol. 40 of NATO Science Series, Kluwer Academic, Dordrecht, the Netherlands, chap. 4, 97–148, 2004.

Gruber, N. and Sarmiento, J. L.: Global patterns of marine nitrogen fixation and denitrification, Global Biogeochem. Cy., 11, 235–266, doi:10.1029/97GB00077, 1997.

Hamersley, M. R., Lavik, G., Woebken, D., Rattray, J. E., Lam, P., Hopmans, E. C., Damsté, J. S. S., Krüger, S., Graco, M., Gutiérrez, D., and Kuypers, M. M. M.: Anaerobic ammonium oxidation in the Peruvian oxygen minimum zone, Limnol. Oceanogr., 52, 923–933, doi:10.4319/lo.2007.52.3.0923, 2007.

Holl, C. M. and Montoya, J. P.: Interactions between nitrate uptake and nitrogen fixation in continuous cultures of the marine diazotroph *Trichodesmium* (cyanobacteria), J. Phycol., 41, 1178–1183, doi:10.1111/j.1529-8817.2005.00146.x, 2005.

Houlton, B, Z, Wang, Y.-P., Vitousek, P, M and Field., C, B: A unifying framework for dinitrogen fixation in the terrestrial biosphere, Nature, 454, 327–331, doi:doi:10.1038/nature07028, 2008.

Kalvelage, T., Lavik, G., Lam, P., Contreras, S., Arteaga, L., Löscher, C. R., Oschlies, A., Paulmier, A., Stramma, L., and Kuypers, M. M. M.: Nitrogen cycling driven by organic matter export in the South Pacific oxygen minimum zone, Nat. Geosci., 6, 228–234, doi:10.1038/NGEO1739, 2013.

Key, R. M., Kozyr, A., Sabine, C. L., Lee, K., Wanninkhof, R., Bullister, J. L., Feely, R. A., Millero, F. J., Mordy, C., and Peng, T.-H.: A global ocean carbon climatology: results from Global Data Analysis Project (GLODAP), Global Biogeochem. Cy., 18, 1–23, doi:10.1029/2004GB002247, 2004.

Kuypers, M. M. M., Lavik, G., Woebken, D., Schmid, M., Fuchs, B. M., Amann, R., Jørgensen, B. B., and Jetten, M. S. M.: Massive nitrogen loss from the Benguela upwelling system through anaerobic ammonium oxidation, P. Natl. Acad. Sci. USA, 102, 6478–6483, doi:10.1073/pnas.0502088102, 2005.

La Roche, J. and Breitbarth, E.: Importance of the diazotrophs as a source of new nitrogen in the ocean, J. Sea Res., 53, 67–91, doi:10.1016/j.seares.2004.05.005, 2005.

Landolfi, A., Dietze, H., Koeve, W., and Oschlies, A.: Overlooked runaway feedback in the marine nitrogen cycle: the vicious cycle, Biogeosciences, 10, 1351–1363, doi:10.5194/bg-10-1351-2013, 2013.

Lenton, T. M. and Watson, A. J.: Redfield revisited 1. Regulation of nitrate, phosphate, and oxygen in the ocean, Global Biogeochem. Cy., 14, 225–248, doi:10.1029/1999GB900065, 2000.

Libby, W. F.: Radiocarbon dating, Am. Sci., 44, 98–112, 1956.

Liu, K.-K. and Kaplan, I. R.: Denitrification rates and availability of organic matter in marine environments, Earth Planet. Sc. Lett., 68, 88–100, doi:10.1016/0012-821X(84)90142-0, 1984.

Martin, J. H., Knauer, G. A., Karl, D. M., and Broenkow, W. W.: VERTEX: carbon cycling in the northeast Pacific, Deep-Sea Res., 34, 267–285, 1987.

McAllister, C. D., Shah, N., and Strickland, J. D. H.: Marine phytoplankton photosynthesis as a function of light intensity: a comparison of methods, J. Fish. Res. Board Can., 21, 159–181, doi:10.1139/f64-010, 1964.

Mills, M. M. and Arrigo, K. R.: Magnitude of oceanic nitrogen fixation influenced by the nutrient uptake ratio of phytoplankton, Nat. Geosci., 3, 412–416, doi:10.1038/NGEO856, 2010.

Mills, M. M., Ridame, C., Davey, M., La Roche, J., and Geider, R. J.: Iron and phosphorus co-limit nitrogen fixation in the eastern tropical North Atlantic, Nature, 429, 292–232, doi:10.1038/nature02550, 2004.

Molina, V. and Farías, L.: Aerobic ammonium oxidation in the oxycline and oxygen minimum zone of the eastern tropical South Pacific off northern Chile ($\sim 20°$ S), Deep-Sea Res. Pt. II, 56, 1032–1041, doi:10.1016/j.dsr2.2008.09.006, 2009.

Monteiro, F. M., Follows, M. J., and Dutkiewicz, S.: Distribution of diverse nitrogen fixers in the global ocean, Global Biogeochem. Cy., 24, 1–16, doi:10.1029/2009GB003731, 2010.

Moore, J. K. and Doney, S. C.: Iron availability limits the ocean nitrogen inventory stabilizing feedbacks between marine denitrification and nitrogen fixation, Global Biogeochem. Cy., 21, 1–12, doi:10.1029/2006GB002762, 2007.

Morrison, J., Codispoti, L., Gaurin, S., Jones, B., Manghnani, V., and Zheng, Z.: Seasonal variation of hydrographic and nutrient fields during the US JGOFS Arabian Sea Process Study, Deep-Sea Res. Pt. II, 45, 2053–2101, doi:10.1016/S0967-0645(98)00063-0, 1998.

Palmer, J. and Totterdell, I.: Production and export in a global ocean ecosystem model, Deep-Sea Res. Pt. I, 48, 1169–1198, doi:10.1016/S0967-0637(00)00080-7, 2001.

Paulmier, A. and Ruiz-Pino, D.: Oxygen minimum zones (OMZs) in the modern ocean, Prog. Oceanogr., 80, 113–128, doi:10.1016/j.pocean.2008.08.001, 2009.

Redfield, A. C., Ketchum, B. H., and Richards, F. A.: The influence of organisms on the composition of sea-water, in: The Sea, 26–77, 1963.

Robarts, R. D. and Zohary, T.: Temperature effects on photosynthetic capacity, respiration, and growth rates of bloom forming cyanobacteria, New Zeal. J. Mar. Fresh., 21, 391–399, doi:10.1080/00288330.1987.9516235, 1987.

Schmittner, A., Oschlies, A., Matthews, H. D., and Galbraith, E. D.: Future changes in climate, ocean circulation, ecosystems, and biogeochemical cycling simulated for a business-as-usual CO_2 emission scenario until year 4000 AD, Global Biogeochem. Cy., 21, doi:10.1029/2007GB002953, 2008.

Shaffer, G. and Sarmiento, J. L.: Biogeochemical cycling in the global ocean 1. A new, analytical model with continuous vertical resolution and high-latitude dynamics, J. Geophys. Res., 100, 2659–2672, doi:10.1029/94JC01167, 1995.

Somes, C. J., Schmittner, A, Galbraith, E. D, Lehmann, M. F., Altabet, M. A, Montoya, J. P, Letelier, R. M., Mix, A. C., Bourbonnais, A. and Eby, M.: Simulating the global distribution of nitrogen isotopes in the ocean, Global Biogeochem. Cy., 24,1–16, doi:10.1029/2009GB003767, 2010.

Suess, E.: Particulate organic carbon flux in the ocean surface productivity and oxygen utilization, Nature, 288, 260–263, doi:10.1038/288260a0, 1980.

Toggweiler, J. R., Dixon, K., and Bryan, K.: Simulations of radiocarbon in a coarse-resolution world ocean model 1. Steady state prebomb distributions, J. Geophys. Res., 94, 8217–8242, doi:10.1029/JC094iC06p08217, 1989.

Tyrrell, T.: The relative influences of nitrogen and phosphorus on oceanic primary production, Nature, 400, 525–531, 1999.

Van Mooy, B. A. S., Keil, R. G., and Devol, A. H.: Impact of suboxia on sinking particulate organic carbon: enhanced carbon flux and preferential degradation of amino acids via denitrification, Geochim. Cosmochim. Ac., 66, 457–467, doi:10.1016/S0016-7037(01)00787-6, 2002.

Voss, M., Dippner, J. W., and Montoya, J. P.: Nitrogen isotope patterns in the oxygen-deficient waters of the Eastern Tropical North Pacidic Ocean, Deep-Sea Res. Pt. I, 48, 1905–1921, doi:10.1016/S0967-0637(00)00110-2, 2001.

Ward, B. B., Devol, A. H., Rich, J. J., Chang, B. X., Bulow, S. E., Naik, H., Pratihary, A., and Jayakumar, A.: Denitrification as the dominant nitrogen loss process in the Arabian Sea, Nature, 461, 78–81, doi:10.1038/nature08276, 2009.

Ye, Y, Völker, C, Bracher, A,Taylor, B. and Wolf-Gladrow., D. A: Environmental controls on N_2 fixation by Trichodesmium in thetropical eastern North Atlantic Ocean—A model-based study, Deep-Sea Res. I, 64, 104–117, doi:10.1016/j.dsr.2012.01.004, 2012.

Table 1. Model variables.

Variables	Units	Description	Equation
Phy_i	$\mu\mathrm{mol\,N\,kg^{-1}}$	Ordinary phytoplankton in box i	Eq. (2)
NF_i	$\mu\mathrm{mol\,N\,kg^{-1}}$	Nitrogen fixers in box i	Eq. (3)
N_i	$\mu\mathrm{mol\,N\,kg^{-1}}$	Nitrate concentration in box i	Eq. (7)
N_{avg}	$\mu\mathrm{mol\,N\,kg^{-1}}$	Average nitrogen concentration	a
P_i	$\mu\mathrm{mol\,P\,kg^{-1}}$	Phosphate concentration in box i	Eq. (8)
P_{avg}	$\mu\mathrm{mol\,P\,kg^{-1}}$	Average phosphorus concentration	b
O_{2i}	$\mu\mathrm{mol\,kg^{-1}}$	Oxygen concentration in box i	Eq. (9)

a $N_{\mathrm{avg}} = \dfrac{(N_U + Phy_U + NF_U)\cdot V_U + N_{UM}\cdot V_{UM} + (N_S + Phy_S + NF_S)\cdot V_S + N_I\cdot V_I + N_D\cdot V_D}{V_U + V_{UM} + V_S + V_I + V_D}$

b $P_{\mathrm{avg}} = \dfrac{\left(P_U + \frac{Phy_U + NF_U}{r_P}\right)\cdot V_U + P_{UM}\cdot V_{UM} + \left(P_S + \frac{Phy_S + NF_S}{r_P}\right)\cdot V_S + P_I\cdot V_I + P_D\cdot V_D}{V_U + V_{UM} + V_S + V_I + V_D}$

Table 2. Parameters of the physical model configurations. The detailed explanations for these parameters are given in Table 3.

Parameter \ Configuration	**STD** RD	VD VDRD	VID **VIDRD** OB **OBRD**	Units
K_{US}	8.44	3.37	3.41	$m\,yr^{-1}$
K_{UM}	1.59	0.40	0.58	$m\,yr^{-1}$
K_H	47 799	50 475	42 938	$m\,yr^{-1}$
A	7.20	7.30	7.22	$m\,yr^{-1}$
B	18.01	19.60	23.07	$m\,yr^{-1}$
g_U	9.87	8.89	9.88	$m\,yr^{-1}$
g_S	2.94	1.42	1.46	$m\,yr^{-1}$

Configurations in bold are the main configurations.

Table 3. Model parameters.

Parameter	Description	Units	Value	Range[(reference)]
r_a	O_2-used/NO_3-produced during organic carbon(OC) oxidation	–	10.6	8.6–10.6[a]
r_c	C/N ratio of OC oxidation	–	6.63	6.63–7.31[a]
f_U	Remineralization ratio in U	–	20 %	[b]
f_S	Remineralization ratio in S	–	20 %	[b]
f_{UM}	Remineralization ratio in UM	–	70 %	[b]
f_I	Remineralization ratio in I	–	70 %	[b]
r_{den}	OC/NO_3^- in denitrification	–	1.02	1.02[a]
r_p	N/P released in OC oxidation	–	16	15–16[a]
μ	Maximum growth rate of Phy	yr^{-1}	91.5	36.5–1861.5[c]
μ_{NF}	Maximum growth rate of NF	yr^{-1}	30.5[e]	65.7–438[d]
M_q	Quadratic mortality	$yr^{-1}(\mu mol\,N\,kg^{-1})^{-1}$	18.25	3.65–18.25[f]
N_h	Nitrate half saturation constant	$\mu mol\,N\,kg^{-1}$	0.5	0.5[g]
P_h	Phosphate half saturation constant	$\mu mol\,P\,kg^{-1}$	0.03125	0.03[h]
L_x	Length of box x	m	see Fig. 1	–
H_x	Depth of box x	m	see Fig. 1	–
K_H	Horizontal exchange	$m\,yr^{-1}$	[n]	157.68–56 765[a]
K_{US}	Vertical mixing between surface and intermediate depth	$m\,yr^{-1}$	[n]	0.79–31.54[a]
K_{UM}	Vertical mixing between intermediate depth and deep ocean	$m\,yr^{-1}$	[n]	0.21–7.88[a]
$A+B$	Upwelling rates	$m\,yr^{-1}$	[n]	23.7–630.7[a]
O_{2U}	Oxygen concentration in U	$\mu mol\,kg^{-1}$	159.54[i]	–
O_{2S}	Oxygen concentration in S	$\mu mol\,kg^{-1}$	198.11[i]	–
g_U	Gas exchange coefficient for U	$m\,yr^{-1}$	[l]	–
g_S	Gas exchange coefficient for S	$m\,yr^{-1}$	[l]	–
λ	Radioactive decay rate for ^{14}C	yr^{-1}	1.21×10^{-4}	1.21×10^{-4} [j]
N_{SD}	Southern boundary nitrate concentration at depth of D	$\mu mol\,kg^{-1}$	32.65	[k]
N_{SI}	Southern boundary nitrate concentration at depth of I	$\mu mol\,kg^{-1}$	10.93	[k]
P_{SD}	Southern boundary phosphate concentration at depth of D	$\mu mol\,kg^{-1}$	2.30	[k]
P_{SI}	Southern boundary phosphate concentration at depth of I	$\mu mol\,kg^{-1}$	0.84	[k]
O_{2SD}	Southern boundary oxygen concentration at depth of D	$\mu mol\,kg^{-1}$	181.37	[k]
O_{2SI}	Southern boundary oxygen concentration at depth of I	$\mu mol\,kg^{-1}$	217.98	[k]

[a] Ranges for r_a, r_c, r_{den}, K_{US}, K_{UM}, K_H, A and B are the same as in Canfield (2006).
[b] The fraction of regeneration above 500 m has been estimated between 92 % (Suess, 1980) and 97 % (Martin et al., 1987). According to Canfield (2006), most likely 60–70 % of the primary production is remineralised in the OMZ. Thus, we define 20 % and 70 % of export production remineralised in the surface boxes and intermediate boxes respectively.
[c] Furnas (1990)
[d] Robarts and Zohary (1987); Capone et al. (1997)
[e] Temperature-corrected maximum growth rate of NF (Breitbarth et al., 2007).
[f] Palmer and Totterdell (2001); Schmittner et al. (2008)
[g] Eppley et al. (1969)
[h] McAllister et al. (1964)
[i] Average 0–100 m O_2 concentrations of the corresponding areas from World Ocean Atlas (2009).
[j] Libby (1956)
[k] Averages of the corresponding areas from World Ocean Atlas (2009).
[l] These parameter values are defined in Table 2.

Table 4. $\Delta^{14}C$ (in ‰) data from GLODAP used for calibration of the model physical parameters.

Box	Lat (S)	Lon (W)	Depth (m)	Data[a]
U	5–15	80–90	0–100	−72.39
UM	5–15	80–90	100–500	−93.28
S	0–20	90–190	0–100	−62.21
I	0–20	90–190	100–500	−81.02
D	0–20	80–190	500–2000	−160.30
SI[b]	20–40	90–190	100–500	−71.02
SD[b]	20–40	80–190	500–2000	−134.4

[a] GLODAP natural ^{14}C data averaged over the respective regions.
[b] SI and SD represent the southern boundary outside the I and D boxes, respectively.

Table 5. Summary of model configurations.

Configuration	Abbreviation	Reduced denitrification rate	O_2, ^{14}C ventilation of D	O_2, ^{14}C ventilation of I	NO_3^-, PO_4^{3-} exchange of D and I
Standard	**STD**				
Reduced-denitrification	**RD**	+			
Ventilation-D	VD		+		
Ventilation-D+Reduced-denitrification	VDRD	+	+		
Ventilation-ID	VID		+	+	
Ventilation-ID+Reduced-denitrification	**VIDRD**	+	+	+	
Open-boundary	OB		+	+	+
Open-boundary+Reduced-denitrification	**OBRD**	+	+	+	+

+ means that the modification applies to this configuration. The configurations in bold are the main configurations in the text, while the others are the sensitivity configurations described in Appendix E. STD is defined in Sections 2.2 and 2.3; in RD, a reduced denitrification rate is applied; VD indicates that the southern boundary of the model domain is partially opened to allow ventilation of O_2 and ^{14}C (but not NO_3^- and PO_4^{3-}) to the D box; VDRD is the configuration when a reduced denitrification rate is applied in VD; VID differs from VD only in that the partially open southern boundary is extended to allow ventilation of O_2 and ^{14}C also into the I box; VIDRD is the configuration when a reduced denitrification rate is applied in VID; in OB, nutrient (NO_3^- and PO_4^{3-}) mixing is added to VID; OBRD is the configuration in which the reduced denitrification rate is added to OB.

Table 6. Denitrification comparison with model-based and observational estimates.

Data/Models	Denitrification ($\mathrm{Tg\,N\,yr^{-1}}$)
OBRD configuration	5.0[c]
Kalvelage et al. (2013)[a]	10.2[c]
DeVries et al. (2013, pers. comm.)[b]	7.0±2.0[c]
Bianchi et al. (2012)[a]	17.6[d]
Somes et al. (2010, pers. comm.)[b]	5.8[c]
Mills and Arrigo (2010)[b]	1.9[c,∗]

[a] observational estimate; [b] model results; [c] ETSP; [d] entire South Pacific; [∗] OMZ value extrapolated to UM box of our model.
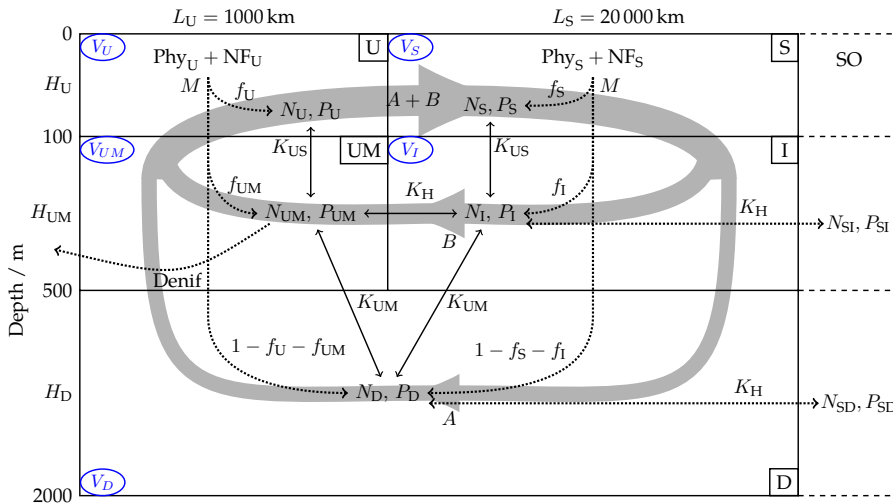
Fig. 1. Model structure and configurations. The model domain comprises five active boxes representing the top 100 m of an upwelling region (U), the underlying oxygen minimum zone (UM), and an adjacent open-ocean basin divided into a surface (S) and an intermediate-depth box (I). A deep box (D) underlies both the upwelling region and the open ocean. The large-scale circulation is represented by deep (A) and shallow (B) convection (thick grey lines). Mixing between boxes is implemented via mixing coefficients (K). Remineralization derived from net primary production by ordinary (Phy) and diazotrophic (NF) phytoplankton in the surface boxes consumes oxygen. Under anoxic conditions remineralization is fueled by anaerobic remineralization (Denif). The model can be configured to exchange nutrients and oxygen with the southern subtropical ocean (right, denoted as "SO"). See Table 3 for symbol definitions and text for details.

37
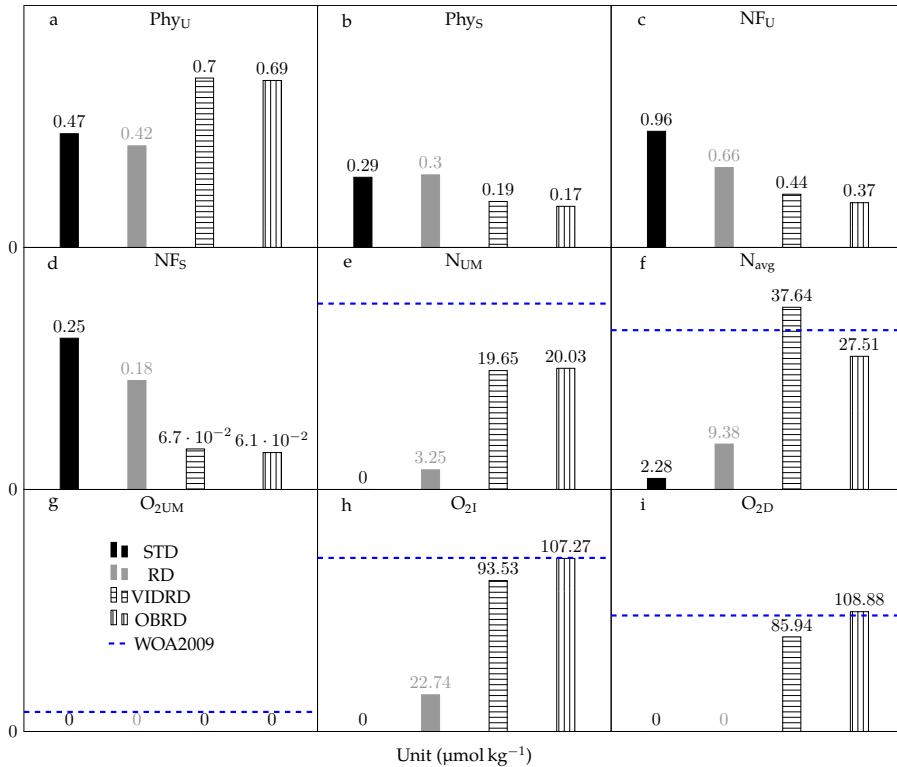
Fig. 2. Simulated steady-state phytoplankton, nutrient and oxygen concentrations for the main model configurations defined in Tables 5 and 2. Each panel uses linear scale of the y-axis starting at zero. Dashed blue lines represent the average of the WOA2009 data of the corresponding boxes, however, there are no data for Phy_U, Phy_S, NF_U and NF_S.
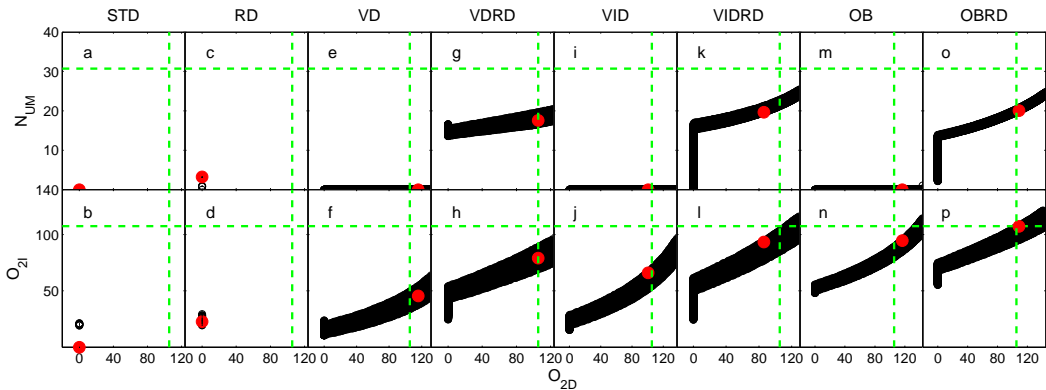
Fig. 3. NO_3^- concentration in the OMZ and O_2 concentrations in the I box for all combinations of g_U and g_S resulting in all transport parameters being inside the literature range as given in Table 3. The x-axis is the O_2 concentration in the D box. Red dot in each panel is the selected suite of physical transport parameters which fit the biogeochemical data best in each model configuration. The horizontal green dashed lines represent the average of WOA2009 data for N_{UM} and O_{2I}, and the vertical green dashed lines denote the average of WOA2009 data for O_{2D}.
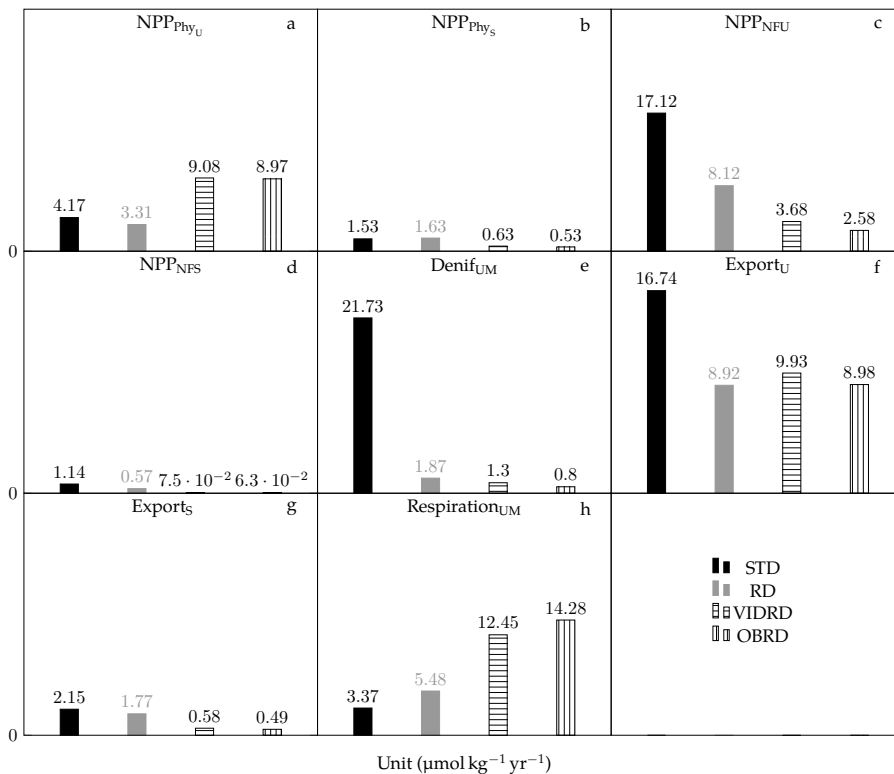
Fig. 4. Simulated steady-state biogeochemical fluxes for the main model configurations defined in Tables 5 and 2. NPP_{PhyU}, NPP_{PhyS}, NPP_{NFU} and NPP_{NFS} represent the net primary production rates of Phy_U, Phy_S, NF_U and NF_S respectively. $Denif_{UM}$ indicates the nitrogen loss rate by anaerobic remineralization in the UM box. $Export_U$ and $Export_S$ represent the export production rate out of U and S. $Respiration_{UM}$ represents aerobic respiration rate in the UM box. Note that all panels are in units of nitrogen except **(h)**, which is in units of O_2. Each panel uses a differrent linear scale for the y-axis starting at zero.

41
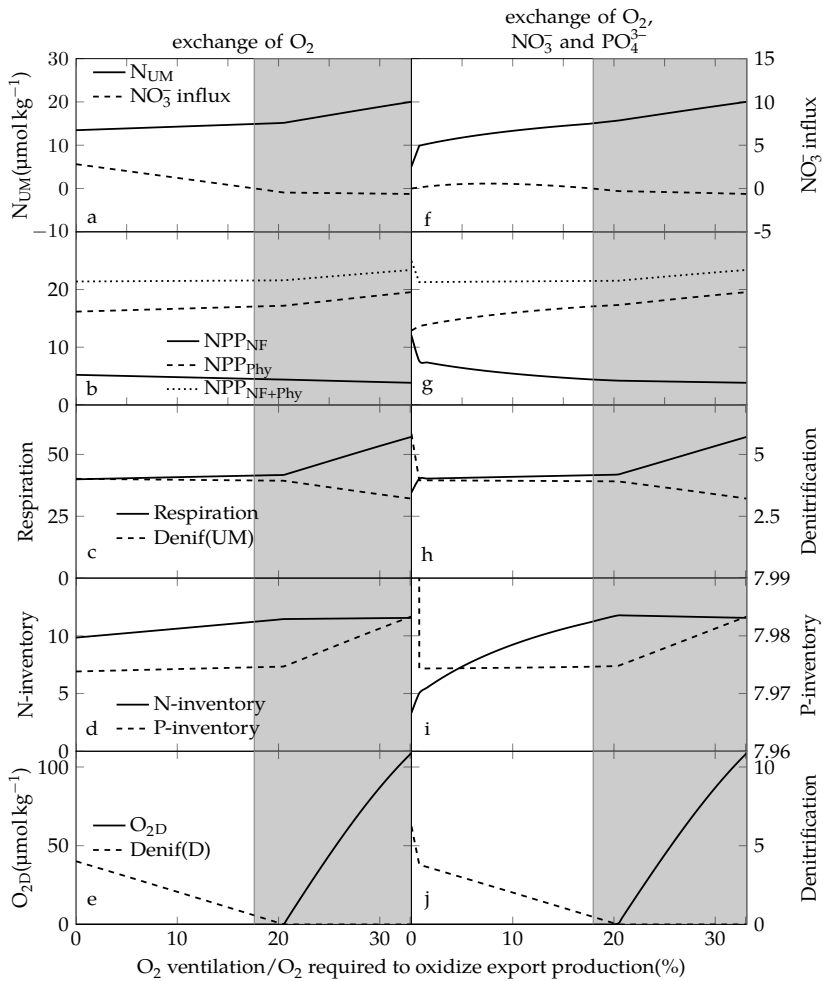
**Fig. 5.** Dependence of biogeochemical processes on the exchange of O_2, NO_3^-, and PO_4^{3-} with the subtropical ocean through the southern boundaries of the I and D boxes. The x-axes indicate the contribution of O_2 supplied from the subtropical ocean relative to that required to oxidise all export production from the surface ocean (boxes U and S). (a–e) only O_2 exchanged through the southern boundaries is reduced; (f–j) exchange of O_2, NO_3^-, and PO_4^{3-} is reduced. N_{UM} is NO_3^- concentration in the UM box and NO_3^- influx is the NO_3^- flux through the southern boundary (positive into model domain). NPP_{Phy}, NPP_{NF} and NPP_{NF+Phy} are net primary production by ordinary phytoplankton, nitrogen fixers, and the sum of both in the surface ocean. Respiration and Denif (UM) represent O_2 consumption by aerobic remineralization and NO_3^- removal by anaerobic remineralization, respectively, in the UM box. N-inventory and P-inventory are the total nitrogen and phosphorus inventories in the model domain, including all organic and inorganic species. O_{2D} and Denif (D) represent O_2 concentration and NO_3^- removal by anaerobic remineralization in the D box. Units of all variables are $10^{11}\,\mu\mathrm{mol}\,\mathrm{yr}^{-1}\,\mathrm{m}^{-1}$ except for N_{UM} and O_{2D}, which are given in $\mu\mathrm{mol}\,\mathrm{kg}^{-1}$, and N-inventory and P-inventory, which are $10^{11}\,\mu\mathrm{mol}\,\mathrm{m}^{-1}$. The shaded area denotes the parameter range for which the model domain is a net source of NO_3^-.

42
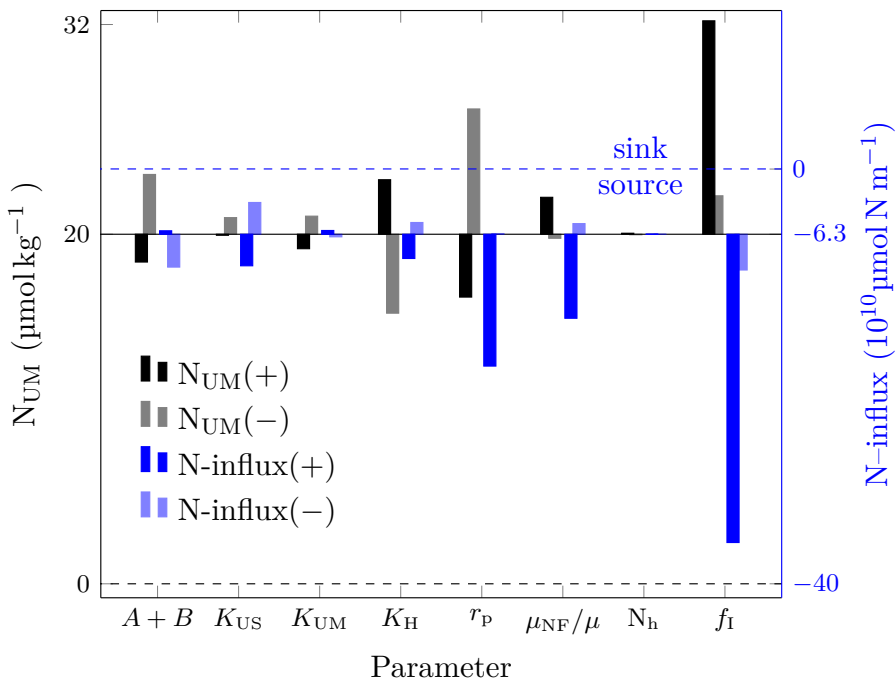
Fig. 6. Sensitivity of NO_3^- concentration in the OMZ (N_{UM}) and the net NO_3^- flux out of the model domain to variations of the individual parameters describing ocean transport and biogeochemical processes (see Tables 2, 3 and Fig. 1 for a description of the parameters). Black and blue bars represent changes in N_{UM} and N-influx, respectively. $+$ and $-$ indicate the response to increased and decreased parameters. Physical circulation parameters are varied by $\pm 50\%$. r_P is varied between 12 and 20. μ_{NF}/μ is varied between 1/4 and 1/2. N_h varies between 0.3 and 0.9 $\mu mol\,kg^{-1}$. For f_i, "+" indicates $f_U = f_S = 60\%$ and $f_{UM} = f_I = 30\%$, and "$-$" means 40% and 50%, respectively.

43
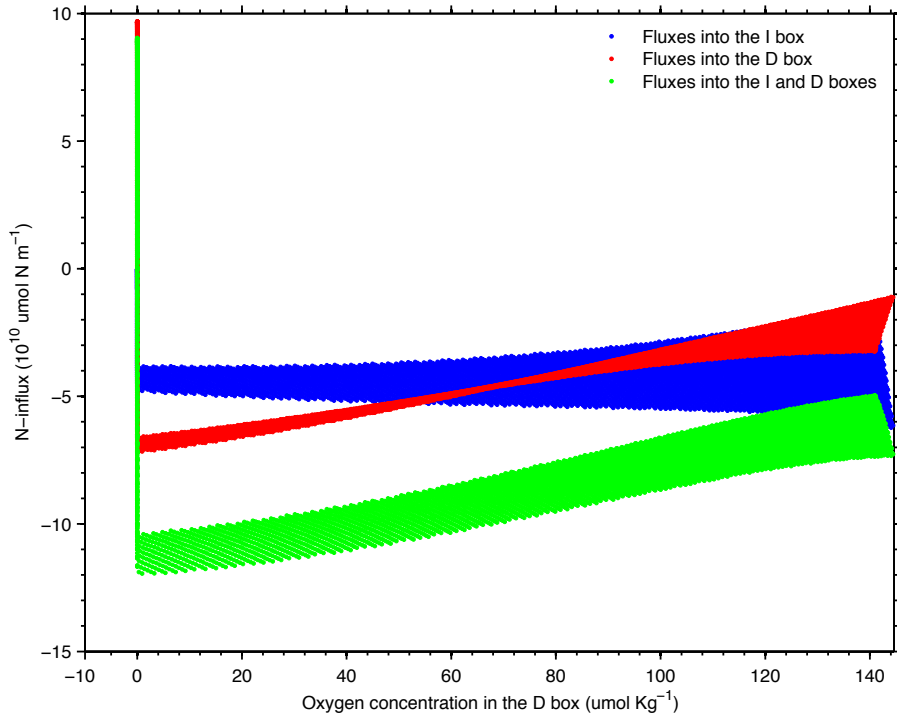
Fig. 7. Lateral NO_3^- input into the model domain of the OBRD configuration as a function of the oxygen concentration in the D box. "Fluxes into the I box" represents lateral NO_3^- input into the I box; "fluxes into the D box" represents lateral NO_3^- input into the D box; "fluxes into the I and D boxes" is the sum of the above two processes. Note that only the I and D boxes can exchange O_2 or nutrients with the region outside of the model domain. In this figure, negative values indicate that the model is a NO_3^- source, and positive values that the model is a NO_3^- sink instead.
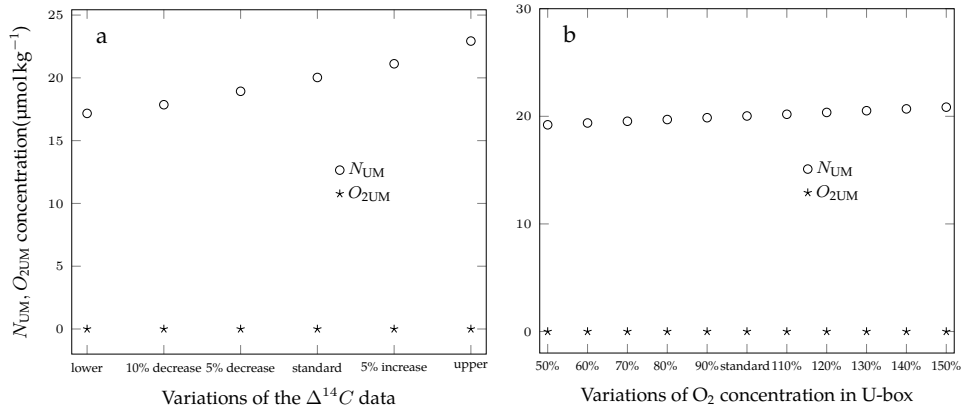
Fig. 8. NO_3^- and O_2 concentrations in the OBRD configuration for different physical parameters derived from variations of the $\Delta^{14}C$ data **(a)** and O_2 concentration in U-box **(b)**. **(a)** Decrease and increase mean that $\Delta^{14}C$ values in all boxes are reduced or increased simultaneously. **(b)** Values of the x-axis denote the variations of O_2 concentration in the U-box relative to the standard. Standard run in each figure is the OBRD configuration with physical parameters defined in Table 2.